Solid Effect Between Quadrupolar Transitions in Dilute Cu-Pd Alloys*

K. Konzelmann, G. Majer, and A. Seeger

Max-Planck-Institut für Metallforschung, Institut für Physik, Heisenbergstraße 1, D-70569 Stuttgart, Germany

Z. Naturforsch. **51a**, 506–514 (1996); received February 13, 1996

The paper investigates the Dynamic Solid Effect (DSE) in Nuclear Quadrupole Double Resonance (NQDOR) on a system (dilute alloys of CuPd with 8, 42, 210, or 1000 at.ppm Pd) chosen for its simplicity and the possibility to test the theoretical concepts on which the experimental techniques (in particular the so-called Berthier-Minier technique for exhibiting the DSE) are based. NQDOR allows to observe the transitions between the Cu nuclear energy levels split by the quadrupolar interaction with the electric field gradients generated by nearby Pd atoms even in dilute alloys, in which the fraction of Cu nuclei experiencing a given field gradient is very small. The DSE permits transitions at frequencies corresponding to the sums or differences of quadrupolar level splittings at neighbouring nuclei and thus gives access to information on the spatial correlation of nuclei accessible to NQDOR studies. The DSE information is shown to be in full accord with the conclusions drawn earlier, on the basis of line-intensity arguments, on the assignment of quadrupolar transitions to the first four shells of Cu nuclei surrounding isolated Pd atoms but, in addition, allows to identify the low-frequency NQDOR lines associated with Cu nuclei in the fifth and sixth shells.

Key words: Nuclear quadrupole double resonance, Atomic defects in Cu, Electric field gradients, Solid effect.

1. Introduction and General Background

In perfect crystals with cubic point symmetry of the lattice sites the electric field gradients (EFG) at these sites vanish. The introduction of lattice defects such as foreign atoms in substitutional solid solution disturbs this symmetry and hence gives rise to non-vanishing EFG at the sites of nearby nuclei. The interaction of these field gradients with nuclear quadrupole moments, Q, leads to a splitting of the nuclear energy levels in the neighbourhood of the defects that is proportional to the EFG and therefore different at crystallographically non-equivalent sites. Each atomic defect is thus characterized by a set of discrete level splittings. However, the nuclei with a given set of splittings are a small minority of all nuclei in the sample. A powerful tool for measuring the quadrupolar level splittings of such minorities is **N**uclear **Q**uadrupolar **D**ouble **R**esonance (NQDOR). It was first employed by Redfield [1] to study substitutional foreign atoms in Cu, and later by the Grenoble group [2–6] and by the present writers and their associates [7–9] to investigate intrinsic atomic defects as well as foreign atoms in Cu and Al. In copper and aluminium, crystal defects even in atomic concentrations as low as a few ppm may be detectable by this technique.

The principal aim of the present study is to investigate the so-called **D**ynamic **S**olid **E**ffect (DSE) in NQDOR in a system that is simple enough to permit independent control of the underlying concepts. The DSE is a well-known phenomenon in magnetic resonance [10, 11]. Its origin lies in the coupling (often but not necessarily dipolar) between different spin systems with level splittings that are large compared to the splitting caused by the coupling interaction. Such a weak coupling mixes the eigenfunctions of the two spin systems and may lead to dynamic polarization phenomena analogous to those well-known in electron paramagnetic resonance as Overhauser effect [12, 13]. The name *Dynamic Solid Effect* takes into account that an essential feature are *dynamic* processes, e.g. simultaneous spin flips, and that dipolar coupling (the main coupling mechanism) is effective only in *solids*, since in fluids it is averaged out by the fast motion of the spin carriers.

* Presented at the XIIIth International Symposium on Nuclear Quadrupole Interactions, Providence, Rhode Island, USA, July 23–28, 1995.

Reprint requests to Dr. G. Majer.

0932-0784 / 96 / 0500-0506 $ 06.00 © – Verlag der Zeitschrift für Naturforschung, D-72072 Tübingen

In NQDOR, the dynamic solid effect permits additional transitions (i.e., transitions which do *not* relate to a well-defined electric field gradient) to appear at sum and difference frequencies (to be denoted by $\nu_{\mathrm{DSE}}^{\pm}$) of transitions which correspond to an electric field gradient. The transitions made possible by DSE will be referred to as "DSE transitions" or "DSE lines". They can be separated from "normal" transitions (sometimes referred to as "EFG transitions" or "EFG lines") by special irradiation techniques that allow us not only to identify those lines which do not correspond to a definitive EFG but also to deduce their frequencies fairly accurately. Since these frequencies are sums or differences of EFG transitions of nuclei close enough for their spin eigenfunctions to be mixed, the DSE lines give information on the spatial correlation of the shells associated with the observed frequencies [14]. In metals such as Cu with several quadrupole-moment-carrying isotopes of different but not too small abundances (the abundances of the two stable isotopes of Cu are 69.1% [^{63}Cu] and 30.9% [^{65}Cu]) DSE lines can be distinguished from EFG lines in a rather straightforward manner owing to the fact that the latter occur always in pairs (or triplets, etc.) with a fixed frequency ratio and an intensity ratio corresponding to the abundance ratio, whereas for the DSE lines this is not so.

The frequencies, and to some extent also the intensity ratios of the EFG lines, constitute "fingerprints" of the defects giving rise to the EFG that may help us to recognize their presence when we do not have a-priori knowledge of the kind of defects involved. A prerequisite for this is, of course, that we have been able to find the correct assignment of the observed lines to definite defect types. Since the EFG transitions involved in a DSE necessarily belong to the same defect, observation of DSE may facilitate the solution of this part of the problem substantially.

The individual EFG lines associated with a given defect type are due to transitions at nuclei that experience EFG tensors with the same principal values. (In zero applied magnetic fields, as in NQDOR, the crystallographic orientation of the axes of the EFG tensor is irrelevant for the quadrupolar level splitting.) This suggests a classification of these nuclei in terms of *shells* of neighbours surrounding the defects. Nuclei belonging to the same shell (or subshell, see below) may be transformed into each other by rotations around or inversion at a suitably chosen defect centre. In many cases (this includes the present case of substitutional foreign atoms as well as vacancies and the so-called dumb-bell self-interstitials, cf. [8]), the appropriate centres are the lattice points, but in other cases (e.g., for divacancies and so-called octahedral self-interstitials [8]) other choices may be appropriate. The nuclei belonging to a given shell have necessarily the same distance from the defect centre, hence we may number the shells according to increasing distances from the centre. If we do this using the distances d_0 in the *ideal* lattice, i.e. *before* the introduction of the defects, we must be aware of the fact that this may not suffice to characterize the shells uniquely. There are, in fact, two different types of complications which must be clearly distinguished.

(i) Not even in the ideal crystal can the atoms at given distances d_0 from a chosen centre always be transformed into each other by rotations or inversions that preserve the crystal structure. An example, with the fcc lattice sites as centres, is referred to in footnote 1; other examples occur when the octahedral interstitial sites of the fcc structure are chosen as centres (cf. [8]). By definition, in such a case we are dealing with several shells, which have to be distinguished accordingly.

(ii) The point symmetry at the centres may be broken by the introduction of the defects. An example for this are dumb-bell self-interstitials. Then nuclei that lay on one shell in the unperturbed crystal will experience different electric field gradients, depending on the crystallographic orientation of their sites with respect to the symmetry-breaking defect. In such a case we may subdivide the original shells into *subshells*. Nuclei belonging to different subshells of a given shell have the same distance from the defect centre in the ideal crystal structure but in general not in that perturbed by the defects. The field gradients acting on nuclei on different subshells may, in fact, be quite different [15].

The number of nuclei belonging to a given shell or subshell is called the *multiplicity* m of that shell or

[1] At the distance $(9/2)^{1/2}\, a_0$ from the lattice points of the fcc structure there lie two shells, with multiplicities 12 and 24 (position vectors $a_0\langle 330\rangle/2$ or $a_0\langle 411\rangle/2$, respectively) [3]. They are *not* subshells of an $n = 9$ shell, since even in the absence of symmetry breaking their sites cannot be transformed into one another by one of the symmetry operations of the octahedral group. This is obvious from the fact that the sum of their multiplicities, $12 + 24 = 36$, is *not* a divisor of 48, the number of elements in the point symmetry group of the lattice sites in the fcc structure.

subshell [8]. From the above definition of shells it follows (a) that the maximum value of the multiplicity is equal to the number of elements in the point group of the sites of the defect centres and (b) that m has always to be a divisor of that number.

The shells around defects in the fcc structure (a_0 = edge length of the elementary cube) whose centres *are* lattice points and whose introduction does *not* break the point symmetry at these points are characterized uniquely by the assignment of a shell number n based on the distance in the ideal lattice according to

$$d_0 = (n/2)^{1/2}\, a_0 \quad (n = 1, 2, 3, \ldots) \tag{1}$$

up to and including $n = 8$ [1]. The multiplicities of the first six shells are given in Table 1, those of shells 7 (position vectors $a_0\langle 321\rangle/2$) and 8 (position vectors $a_0\langle 400\rangle/2$) are $m = 48$ and $m = 6$, respectively. (Since the octahedral group has 48 elements, the seventh shell thus provides an example of the maximum multiplicity possible.)

The assignment of the EFG lines to shells (or subshells), which is necessary, e.g., for critical comparisons between computations of EFG and experiments, is facilitated on the one hand by the trend that (barring exceptions due to the oscillatory character of the Friedel oscillations [16]) the electric field gradients decrease with increasing distance from the defects and on the other hand by the qualitative (in the DIT regime – see Sect. 2 – even quantitative) relationship between line intensity and shell multiplicity [8]. (E.g., the nearest-neighbour shell of substitutional atoms in a face-centred cubic metal has the multiplicity 12. It should therefore give rise to a stronger NQDOR line than the next-nearest-neighbour shell, which has the multiplicity 6.)

The DSE may be used to test the correctness of the assignments obtained by the arguments just outlined. As already mentioned, DSE transitions must belong to the same kind of defect. Therefore, if two different DSE have one of the EFG transitions in common, we may conclude that the other two EFG transitions involved must belong to the same defect, too, even if they do not combine to give an observable DSE transition. – Further, the nuclei participating in a DSE transition must be nearest or next-nearest neighbours of each other, since otherwise the coupling is too weak. This condition can be quite stringent in the case of defects with low point symmetry. For defects in fcc metals that are located at lattice sites and maintain the cubic point symmetry of these points, the structural information on nearest and next-nearest neighbour pairs up to the 8th shell is collected in Table 2. Here each shell is represented by a column and a line. The entries above the diagonal line give the number of the nearest-neighbour pairs between the two shells, those below the diagonal that of the next-nearest-neighbour pairs. The fields on the main diagonal contain the

Table 1. Shell numbers, position vectors of the sites on the shells in the ideal fcc lattice measured from the Pd site (in units of $a_0/2$), multiplicities m of the shells (in italics if the EFG tensor is axially symmetric by symmetry), number and measurement regime of the EFG line pairs in Pd-doped Cu attributed to the shell, frequencies of the ^{63}Cu lines as measured on a 300 at.ppm Pd alloy (Minier and Minier [3], frequencies taken from their Fig. 2) and on an 42 at.ppm Pd alloy (present work). The frequencies of the ^{65}Cu lines are smaller by a factor of 1.079. M^* denotes the logarithm of the intensity of the NQDOR lines in the 42 at.ppm alloy, M^*/M^* (pair II) its normalization to the intensity of the line pair II.

Shell number n	1	2	3	4	5	6
Position vectors $[a_0/2]$	$\langle 110\rangle$	$\langle 200\rangle$	$\langle 211\rangle$	$\langle 220\rangle$	$\langle 310\rangle$	$\langle 222\rangle$
Multiplicity m	12	*6*	24	12	24	*8*
Pair number	I	II	IV	III	V	VI
Measurement regime	DIT	DIT	DIT	DIT	SIT	SIT
ν (300 at.ppm Pd) [kHz]	3150	525	240	400	–	–
ν (42 at.ppm Pd) [kHz]	3145 ± 3	534 ± 3	241 ± 3	404 ± 3	65 ± 5	55 ± 5
M^* [arb. units]	7.9	5.6	21.1	11.0	–	–
M^*/M^* (pair II)	1.4	1.0	3.8	2.0	–	–

Table 2. Numbers of nearest-neighbour (above diagonal) or next-nearest-neighbour (below diagonal) pairs *on* the shells (diagonal fields) or *between* different shells (off-diagonal fields) surrounding an fcc lattice site. The shell numbers n are shown in italics.

n	*1*	*2*	*3*	*4*	*5*	*6*	*7*	*8*
1	12 / 24	24	48	12	0	0	0	0
2	0	0 / 0	24	0	24	0	0	0
3	24	0	24 / 24	48	48	24	48	0
4	0	24	0	0 / 0	24	0	48	0
5	24	0	0	0	12 / 24	0	48	24
6	0	0	0	24	0	0 / 0	48	0
7	0	0	48	0	48	0	24 / 48	0
8	0	6	0	0	0	0	0	0 / 0

numbers of nearest (above the line) or next-nearest (below the line) neighbours within the same shell. – Finally, identification of an DSE line can assist us in getting accurate frequency values for EFG transitions in the low-frequency regime, where lines are likely to overlap and where the relative accuracy of the frequency determination is not very high.

In view of the importance the DSE for the correct interpretation of NQDOR measurements on complicated systems, it appeared highly desirable to study the effect on a simple system on which a convincing shell assignment already exists. Dilute CuPd alloys are such a system. In contrast to most experiments on *intrinsic* atomic defects, in this system there is no doubt that the EFG acting on the Cu nuclei are due to Pd atoms. Furthermore, in sufficiently dilute alloys we can be sure that the majority of the solute Pd atoms are isolated atoms on lattice sites. The lattice sites occupied by such isolated Pd atoms are points of octahedral point symmetry, hence the classification of the Cu nuclei in the neighbourhood of the Pd atoms according to their distance from the Pd atoms as belonging to the first (= nearest neighbour), second (= next-nearest neighbour) etc. shells is applicable.

The quadrupolar splitting of the energy levels of the two stable Cu isotopes (^{63}Cu and ^{65}Cu, both with spin 3/2, with quadrupole-moment ratio $Q(^{63}\mathrm{Cu})/Q(^{65}\mathrm{Cu}) = 1.0790 \pm 0.0015$ [3]) around substitutional Pd has been investigated before. The quadrupolar frequencies determined on a $\mathrm{CuPd}_{0.0003}$ powder specimen by Minier and Minier [3] by means of NQDOR for the first four shells are included in Table 1 [2]. The transition frequency of the first shell as deduced by Nevald and Petersen [17] on $\mathrm{CuPd}_{0.01}$ from the dependence of the NMR satellite lines on the crystallographic orientation of the external magnetic field, $\nu_q = (3100 \pm 50)$ kHz, agrees with the Minier-Minier value within experimental uncertainty. In addition, Nevald and Petersen [17] determined the anisotropy parameter of the EFG tensor associated with this transition as $\eta = 0.19 \pm 0.03$. In their Table 2 Minier and Minier [3] made a tentative assignment of low-frequency lines to more distant shells on the basis of intensity ratios, namely 68 kHz to $n = 5$, 35 kHz to $n = 6$, 25 kHz to $n = 8$, and 57 kHz to one of the two $n = 9$ shells.

The present paper reports on NQDOR studies of Cu samples doped with 8, 42, 210 and 1000 at.ppm Pd, with particular reference to the Dynamic Solid Effect. Sect. 2 presents the NQDOR data on these four compositions and compares them with the earlier measurements. In Sect. 3 the DSE studies performed on the same samples will be reported and discussed in some detail. In a final section (Sect. 4) the results of the present study will be summarized with special emphasis on the conclusions that may be drawn by combining the information from the NQDOR measurements with that obtained by the DSE investigations.

[2] All frequencies are for ^{63}Cu.

2. NQDOR Measurements

NQDOR is based on an idea due to Ramsey [18] and was first applied to metals by Anderson [19], who mentioned Redfield's suggestion to use it for the direct observation of quadrupole lines. In a field-cycling NQDOR experiment the sample is first polarized in a static high magnetic field. Then the field is switched off adiabatically and a radio frequency (r.f.) is applied in zero magnetic field in order to scan the distribution of level splittings. At low quadrupolar frequencies the cross-relaxation between the quadrupolar reservoir of the spins in the vicinity of lattice defects and the dipolar reservoir of the spins at sites far from any lattice defect is sufficiently effective to maintain the thermal equilibrium. Therefore, the polarization and hence the NMR signal is reduced when the r.f. in zero field matches a quadrupolar transition. In this regime of the so-called Single Irradiation Technique (SIT) r.f. irradiation with only one single frequency of low amplitude $B_1^{\mathrm{NQR}} \ll B_L$ (B_L: local magnetic field) suffices to continually heat all spins of the sample. At higher frequencies the cross-relaxation becomes ineffective and the quadrupolar reservoir is thermally isolated. Hence, simultaneous irradiation with large amplitudes $B_1^{\mathrm{NQR}} \approx B_L$ at two frequencies $\nu_q \pm \delta\nu$ near the quadrupolar transition frequency ν_q is required in order to achieve continual heating of the entire spin system. In this so-called Double Irradiation Technique (DIT) regime a quantitative analysis of the NQDOR line intensities is possible [8]. The work of Redfield [1], who was the first to measure EFG in dilute copper alloys by means of the two NQDOR techniques, and of Minier [5], who applied the method to dilute aluminium alloys, demonstrated that the spectra observed by these techniques are indeed characteristic for specific substitutional atoms.

Figure 1 shows SIT spectra measured on four Cu samples with different Pd content. Owing to the strong dipolar background in the low-frequency regime, in the frequency range covered by Fig. 1 the NQDOR lines are not well resolved. This dipolar background increases with increasing defect concentration. The resolution is clearly not good enough to separate the ^{63}Cu and ^{65}Cu lines from each other. The NQDOR frequencies that may be deduced from the SIT spectra depend therefore slightly on the concentration of substitutional atoms. In the sample with 42 ppm Pd NQDOR lines have been observed at 35, 55 and 67 kHz with uncertainties of about $\pm$ 5 kHz.

DIT spectra of the four samples are shown in Figures 2 and 3. For clarity the curves have been shifted with increasing Pd concentration by 5% each in Fig. 2 and by 2% each in Figure 3. The spectra indicate four well-resolved pairs of NQDOR lines, numbered I to IV. In each pair the line at the higher frequency is about twice as high as that at the lower frequency, reflecting the abundance ratio 2.24 of the two isotopes ^{63}Cu and ^{65}Cu. In addition to these line pairs, the spectra show weak lines at about 310 kHz and 470 kHz. Because of the absence of a pair structure, these lines are candidates for DSE lines. They will be discussed in Sect. 3. In the frequency range between 600 kHz and 2.85 MHz no NQDOR transitions were observed.

The frequencies given in Table 1 have been obtained by fitting Lorentzian lines to the spectra. The M^*-values denote the logarithms of the signal intensities measured on Cu-42 ppm Pd. Unless the defect concentration exceeds several 100 ppm, M^* is proportional to the number of nuclei with the same quadrupolar splitting and, assuming random distribution of the two isotopes, hence to the number m of nuclei in a shell.

By ab-initio computations of the electric field gradient and the anisotropy parameter η at the nearest-neighbour nuclei of a substitutional Pd atom in Cu, employing the Full-Potential Linearized-Augmented-Plane-Wave (FLAPW) method [20] for a 16-atom supercell, and using the quadrupole moment $Q = -220 \cdot 10^{-31}$ m^2, Ehmann [15] has recently calculated the corresponding EFG frequency of ^{63}Cu,

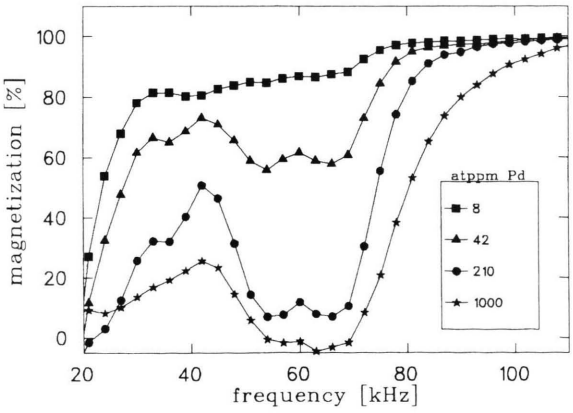

Fig. 1. NQDOR spectra of dilute copper alloys with 8, 42, 210 and 1000 at.ppm Pd, obtained in the SIT regime using r.f. irradiation with $B_1^{NQR} = 0.016$ mT.

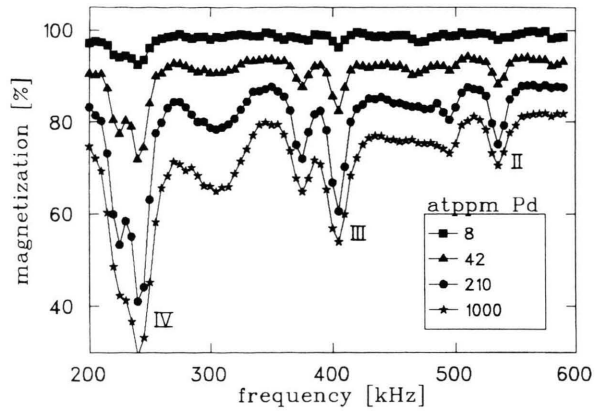

Fig. 2. NQDOR spectra of dilute copper alloys with different Pd concentrations, obtained in the DIT regime using r.f. irradiation with $B_1^{NQR} = 1.6$ mT (at two slightly different frequencies). In order to avoid overlap, the spectra have been shifted by 5% each with increasing Pd concentration.

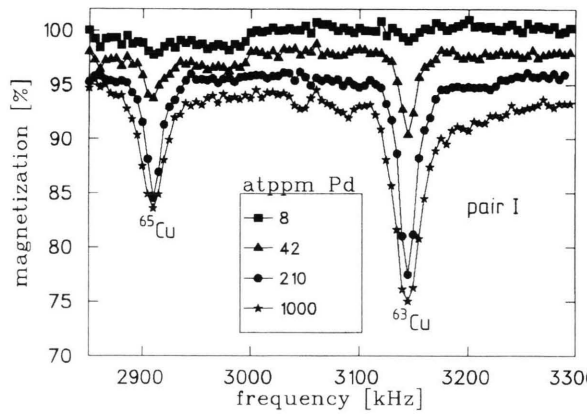

Fig. 3. The upper DIT regime of dilute copper alloys with different Pd concentrations, obtained with $B_1^{NQR} = 1.6$ mT. The spectra have been shifted by 2% each with increasing Pd concentration.

$\nu_{EFG} = 3.3$ MHz. Although the rather small supercell size limits the accuracy of the result (this applies in particular to the η value), it allows us, nevertheless, to ascribe the line pair with the ^{63}Cu line at 3.145 MHz (line pair 1, cf. Table 1) unambiguously to the first shell. This assignment is in agreement with the results of Nevald and Peterson [17] that the EFG tensor associated with this line is not axially symmetric (which excludes, e.g., the assignment to the shell of next-nearest neighbours).

Since in the DIT regime the signal intensities M^* normalized to the M^*-value of one particular pair are expected to reflect the ratios of the number of nuclei in the different shells, on the basis of the observed ratios $M^*(3)/M^*(2) = 2$ and $M^*(4)/M^*(2) \approx 4$ the line pairs II, III, and IV may be ascribed to the shells 2, 4, and 3, respectively (cf. Table 1). The reduced line intensity due to the nuclei in the first shell is presumably due to the smaller r.f. penetration depth $\delta_{r.f.}$ at high frequency ($\delta_{r.f.} \approx 5$ μm at 3 MHz in Cu/42 ppm Pd at 2.1 K).

The line assignments of Minier and Minier [3], also arrived at by line-intensity arguments, were the same as those of the peceding paragraph for shells 1 to 4. As pointed out in Sect. 1, in the SIT regime, i.e. for the remaining lines, there is no direct relationship between intensity and multiplicity. Therefore the assignments of Minier and Minier [3] of the SIT lines have to be considered with utmost caution. It is in this regime that the DSE is invaluable for line assignment. As we shall see, in the present case it does lead to an assignment that differs from that of Minier and Minier [3].

3. Dynamical Solid Effect

Figure 4 reproduces, as a full line, the DIT measurements on Cu/210 ppm Pd in the frequency interval 150–600 kHz, and compares them with those of a *single-frequency* irradiation with an amplitude B_1^{NQR} as large as that used in DIT. Whereas the well-resolved DIT pairs do not show up in SIT measurements, the weaker absorptions at about 310 kHz and 470 kHz appear also in the single-frequency measurements. Together with the fact that these absorption lines do not exhibit the typical ^{63}Cu/^{65}Cu pair structure, this demonstrates clearly that they are *not* EFG lines and suggests that they might be due to DSE transitions. The correctness of this suggestion may be tested by the following procedure, first applied by

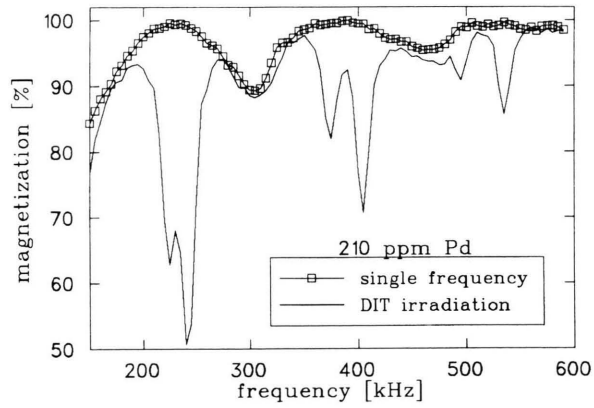

Fig. 4. Two NQDOR spectra of Cu doped with 210 ppm Pd, obtained in the DIT regime using r.f. irradiation with a *single* frequency or with normal DIT with $B_1^{NQR} = 1.6$ mT in both cases.

Berthier and Minier [6] in their NQDOR work on dilute Al alloys.

Perform a low-amplitude NQR irradiation at the higher one of the two EFG frequencies supposed to be involved in the DSE simultaneously with irradiating with a higher amplitude at search frequencies sweeping the frequency range under study. If the absorption structure to be investigated is due to EFG transitions, there will be no change compared with single-frequency irradiations, since in the absence of DSE the two transitions do not influence each other. If, however, the search frequency happens to coincide with a DSE transition, enhanced absorption (= a drop in magnetization) will be observed since the irradiation with the EFG frequency is destroying the polarization associated with the EFG transition. The result is a characteristic "butterfly structure" in the magnetization vs. search-frequency spectrum, with resonance lines at the sum and difference frequencies (to be denoted by $\nu_{DSE}^{\pm}$) of the two EFG lines involved in the Dynamic Solid Effect. In the following we shall illustrate this technique by measurements on the alloy containing 210 ppm Pd.

The specimen was irradiated in zero applied magnetic field with one of the ^{63}Cu EFG frequencies in the DIT regime (in the following to be denoted by ν_{DIT}) at an amplitude $B_1 = 0.28$ mT; simultaneously the frequency range of interest was swept with a search frequency ν_{search} with amplitude $B_1 = 1.4$ mT. "Butterfly patterns" indicative of DSE as discussed above were found for all the ^{63}Cu DIT lines of Table 1. Since from

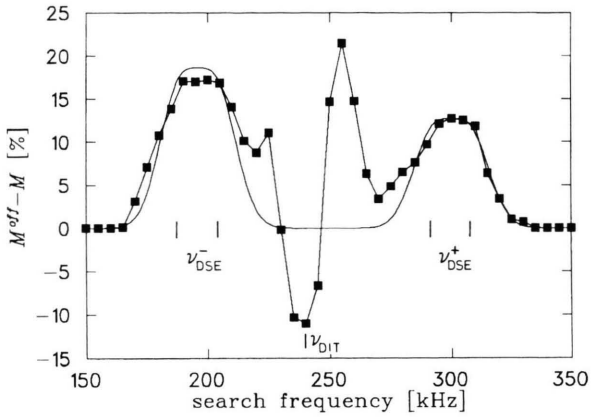

Fig. 5. Reduction of the magnetization as a function of the search frequency to demonstrate the Dynamic Solid Effect on a dilute copper alloy with 210 ppm Pd. ν_{DSE}^{+} and ν_{DSE}^{-} are the frequencies of DSE transitions associated with the DIT line at $\nu_{DIT} = 241$ kHz. At the low *and* at the high-frequency side, the absorption consists of two overlapping lines, indicating a dipolar coupling with the SIT lines at 55 kHz *and* at 65 kHz.

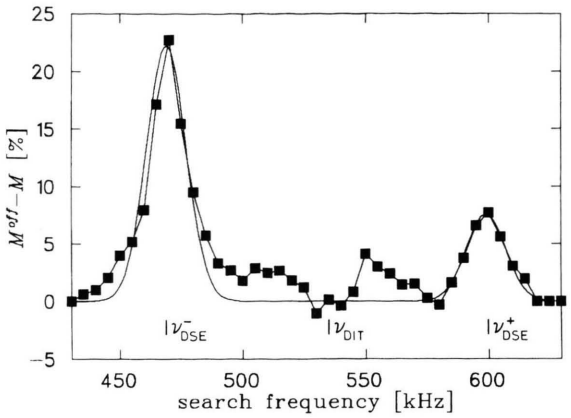

Fig. 7. DSE absorption of Cu/210 ppm Pd. The spectrum indicates DSE lines at $\nu_{DSE}^{-} = (534 - 65)$ kHz and $\nu_{DSE}^{+} = (534 + 65)$ kHz.

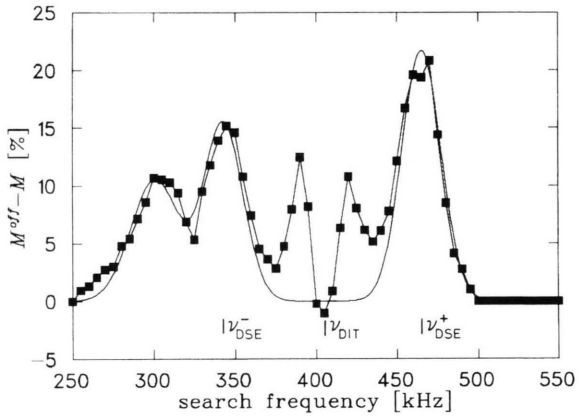

Fig. 6. DSE absorption of Cu/210 ppm Pd. The spectrum indicates overlapping DSE lines at $\nu_{DSE}^{+} = (241 + 55)$ kHz and $\nu_{DSE}^{+} = (241 + 65)$ kHz, as well as resolved DSE lines at $\nu_{DSE}^{-} = (404 - 65)$ kHz and $\nu_{DSE}^{+} = (404 + 65)$ kHz.

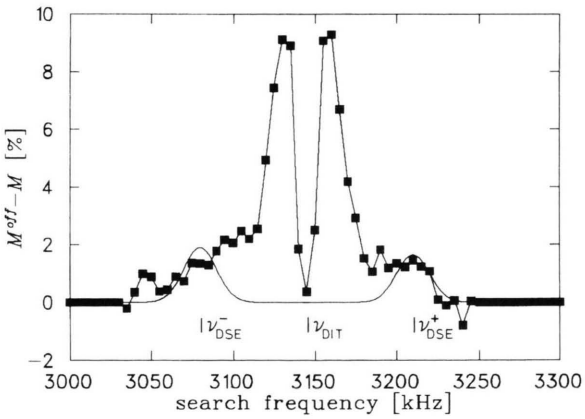

Fig. 8. DSE absorption of Cu/210 ppm Pd. The spectrum indicates DSE lines at $\nu_{DSE}^{-} = (3145 - 65)$ kHz and $\nu_{DSE}^{+} = (3145 + 65)$ kHz.

Figs. 5 to 8 it is apparent that the second transitions involved in the DSE lie in the SIT regime, we write the frequencies of the DSE transitions as

$$\nu_{DSE}^{\pm} = \nu_{DIT} \pm \nu_{SIT} \,. \tag{2}$$

Table 3 gives the DSE frequencies as obtained by Gaussian fits to the experimental data of Figures 5 to 8. Since the butterfly wings associated with the 241 kHz DIT line were broader than the others, we suspected that here we were dealing with the superposition of at least two DSE, hence we employed a superposition of two Gaussians in the fit. The relative uncertainties in the signal intensities are estimated as 0.1, the uncertainties of the ν_{DSE} values as $\pm$ 4 kHz with the exception of the frequency ν_{DSE}^{-} associated with $\nu_{DIT} = 241$ kHz, which is less certain because of the

Table 3. Frequencies ν_{DSE} and line intensities M_{DSE} of the DSE lines identified on a Cu 210 at.ppm Pd alloy. The superscripts 55 of 65 indicate whether the participating transitions in the SIT regime are those at $\nu_{SIT} = 55$ kHz or 65 kHz. The ^{63}Cu frequencies ν_{DIT} of the participating DIT transitions are shown in the top line; the signs underneath indicate the sign obtaining on the left-hand side of (2). For the fitting procedures applied to Figs. 5 to 8. For the estimated uncertainties of the DSE frequencies and intensities see text. The asterisks indicate frequencies that are less certain owing to overlap with the low-frequency dipolar background.

^{63}Cu ν_{DIT} [kHz]	241		404		534		3145	
DSE transition	−	+	−	+	−	+	−	+
ν^{55}_{DSE} [kHz]	204*	292	–	–	–	–	–	–
M^{55}_{DSE} [%]	16.5	9.4	–	–	–	–	–	–
ν^{65}_{DSE} [kHz]	188*	306	343	465	469	599	3080	3210
M^{55}_{DSE} [%]	10.2	9.5	16.4	21.8	21.1	7.6	1.9	1.6

overlap with the low-frequency absorption background due to dipolar interactions. Its uncertainty in estimated to be about ± 15 kHz.

In order to account for the data of Table 3 we need to invoke only two transitions in the SIT regime, with frequencies $\nu_{SIT} = 55$ kHz and 65 kHz. Accordingly, we have labelled the information in Table 3 on the DSE lines (frequency and intensity) by superscripts 55 and 65. As may be seen from Table 2, three of the first four shells (viz. shells No. 2, 3, and 4) have nearest neighbours in the 5th shell, whereas only the 3rd shell has, in addition, nearest neighbours in the 6th shell. Shell No. 1 does not have any nearest neighbours outside the DIT regime, hence any DSE line involving $\nu_{DIT} = 3145$ kHz and a SIT transition should be rather weak. We see immediately that the assignment of $\nu_{SIT} = 65$ kHz to the 5th shell and of $\nu_{SIT} = 55$ kHz to the 6th shell accounts perfectly for the experimental data of Table 3, including the weakness of the DSE lines associated with $\nu = 3145$ kHz.

4. Discussion and Conclusions

The main aim of the present work was to study the **D**ynamic **S**olid **E**ffect (DSE) in **N**uclear **Q**uadrupole **D**ouble **R**esonance (NQDOR) on a system that was simple enough to allow the underlying theoretical ideas to be critically tested, and to explore possible applications of NQDOR-DSE. Experiments on a series of dilute CuPd alloys (8, 42, 210, 1000 ppm Pd) have demonstrated the power of the Berthier-Minier simultaneous-irradiation technique for locating and investigating DSE transitions arising from the combination of an EFG transition in the frequency regime accessible to the double-irradiation technique (DIT) with one in the SIT (single-irradiation technique) regime. It has been shown that if there are several DSE lines involving the same DIT transition, the relationship Eq. (2) between the frequencies ν_{DSE}, ν_{SIT}, and ν_{DIT} may be used to determine ν_{SIT} more reliably than is possible by a direct SIT measurement.

Observation of a DSE frequency ν_{DSE} immediately provides us with information on the spatial correlation of the nuclei giving rise to the frequencies on the right-hand side of Eq. (2). It has been shown that the line intensities obtainable by the Berthier-Minier technique permit next-nearest-neighbour relationships to be distinguished from nearest-neighbour relationships. In the particular case of dilute CuPd alloys investigated in the present work, the analysis of the DSE measurements not only confirmed the conclusions on the assignment of the four DIT transitions observed in "ordinary" NQDOR measurements to the first four shells of Cu neighbours surrounding a substitutional Pd atom but also allowed us to assign reliably two of the quadrupolar frequencies observed in the SIT regime, viz. $\nu_{SIT} = 65$ kHz to the 5th shell and $\nu_{SIT} = 55$ kHz to the 6th shell. Such an assignment of line in the SIT regime does not appear possible in any other way since here no simple relationship between

Table 4. Assignment of the NQDOR frequencies (in kHz) of dilute CuPd alloys to shells (italic numbers) around isolated Pd atoms. The ^{63}Cu EFG frequencies are given on the main diagonal; the entries in the off-diagonal fields on the upper right-hand side correspond to the DSE frequencies resulting from the + sign in Eq. (2), those on the lower left-hand side pertain to the − sign (cf. Table 3). The asterisks denote values with reduced accuracy (see text).The dashes indicate pairs of shells without nearest or next-nearest neighbours.

n	*1*	*2*	*3*	*4*	*5*	*6*
1	3145				3210	–
2		534			599	–
3			241		306	292
4				404	465	
5	3080	469	188*	343	65	–
6	–	–	204*		–	55

line intensity and multiplicity exists. Our assignment differs indeed from that of Minier and Minier [3], which is incompatible with the DSE data. A summary of all our line assignments is given in Table 4.

The third line observed by SIT, with frequency $\nu_q = 35$ kHz, did not show up in our Berthier-Minier tests. This may either mean that it is associated with a shell that does not have nearest neighbours on any of the first *four* shells (candidates are thus the 8th shell and the 9th shell with $m = 24$) or that the high amplitude of the search frequency enhances the background absorption due to dipolar transitions to such an extent that DSE due to the 35 kHz line cannot be detected by the Berthier-Minier technique.

The Berthier-Minier technique as employed in the present work, based on simultaneous irradiation with *two* frequencies, cannot reveal DSE involving two DIT transitions. The study of the DIT–DIT dynamic solid effect would require, in addition to the high-intensity irradiation with the search frequency, simultaneous weak irradiation at both DIT frequencies. The considerable extension of the experimental arrangement necessary for such investigations was not attempted in the present work.

Acknowledgements

During the final work on this paper one of the authors (A. S.) held a Gledden Senior Visiting Fellowship at the Department of Mechanical and Materials Engineering of the University of Western Australia. He should like to thank the University for the award of the fellowship and the department staff for their hospitality and support. The authors also want to express their thanks to Dr. M. Notter for his help and advice during the measurements, and to Professor M. Fähnle and J. Ehmann for providing valuable information on the calculation of electric field gradients in metals.

[1] A. G. Redfield, Phys. Rev. **130,** 589 (1963).
[2] M. Minier, R. Andreani, and C. Minier, Phys. Rev. B **18,** 102 (1978).
[3] M. Minier and C. Minier, Phys. Rev. B **22,** 21 (1980).
[4] M. Minier, C. Minier, and R. Andreani, Phys. Rev. B **22,** 28 (1980).
[5] M. Minier, Phys. Rev. **182,** 437 (1969).
[6] Cl. Berthier and M. Minier, Phys. Rev. B **7,** 1854 (1973).
[7] M. Blanz, M. Hampele, G. Majer, M. Notter, and A. Seeger, in: Congress Ampere on Magnetic Resonance and Related Phenomena (M. Mehring, J. U. Schütz, and H. C. Wolf, eds.), Springer-Verlag, Berlin 1990, p. 38.
[8] M. Notter, K. Konzelmann, G. Majer, and A. Seeger, Z. Naturforsch. **49a,** 47 (1994).
[9] K. Konzelmann, G. Majer, M. Notter, and A. Seeger, Phil. Mag. Lett. **70,** 23 (1994).
[10] A. Abragam, The Principles of Nuclear Magnetism, Clarendon Press, Oxford 1961, England.
[11] M. Goldman, Spin Temperature and Nuclear Magnetic Resonance in Solids, Clarendon Press, Oxford 1970, England.
[12] A. W. Overhauser, Phys. Rev. **91,** 476 (1953).
[13] A. W. Overhauser, Phys. Rev. **92,** 411 (1953).
[14] M. Notter and A. Seeger, The NQI Newsletter **1** (3), 16 (1994).
[15] A. Seeger, J. Ehmann, and M. Fähnle, Z. Naturforsch., **51a,** (1996) in press.
[16] J. Friedel, Adv. Phys. **3,** 446 (1953).
[17] R. Nevald and G. Petersen, J. Phys. F: Metal Phys. **5,** 1778 (1975).
[18] N. F. Ramsay and R. V. Pound, Phys. Rev. **81,** 278 (1951).
[19] A. G. Anderson, Phys. Rev. **115,** 863 (1959).
[20] P. Blaha, K. Schwarz, and P. H. Dederichs, Phys. Rev. B **37,** 2792 (1988).